ELSEVIER

Chemical Engineering Journal 83 (2001) 67–78

Chemical Engineering Journal

www.elsevier.com/locate/cej

Characteristics of turbulence in a multigrid mixer

D.H. Bache*, E. Rasool

Department of Civil Engineering, University of Strathclyde, John Anderson Building, Glasgow G4 ONG, UK

Received 28 February 2000; received in revised form 2 June 2000; accepted 7 June 2000

Abstract

The paper describes an experimental investigation to determine the distribution and controls on the rate of energy dissipation per unit mass (ε) in an oscillatory multigrid mixer. The study centred on the evaluation of the parameter γ which was treated as a spatial invariant in the expression $\varepsilon = \gamma U^2/\tau_E$ in which U^2 signifies a turbulence intensity and τ_E the Eulerian time scale. This was achieved by using an energy balance, involving the measured power input and the energy losses. When grids were widely spaced, it was evident that the turbulence field was characterised by two principal zones of behaviour. In an internal zone, corresponding to the domain swept by an individual grid, U^2 attained high values compared with other regions and τ_E was essentially constant. Outside this region, the 'external zone', turbulence was characterised by a constant Reynolds number specified by $R_{\Gamma 0} = U_0^2\tau_{E0}/\nu$ in which U_0^2 and τ_{E0} were scaling parameters and ν the kinematic viscosity. It was shown that γ could be defined in terms of the far distance behaviour using the relationship $\gamma \propto R_{\Gamma 0}/R_{\lambda 0}^2$ with $R_{\lambda 0} = \lambda_0 U_0/\nu$ as a turbulence Reynolds number involving the Taylor microscale λ_0. From an energy balance it was shown that $R_{\lambda 0}^2 \propto \sigma R_N^\alpha R_S^{2\beta+1}$ with the Reynolds number $R_N = fSd/\nu$, $R_S = fS^2/\nu$ specifying the grid motion, the terms f, S, d and σ referring to the grid frequency, stroke length, bar diameter and grid solidarity, respectively. Coefficients α and β were linked to the Reynolds number dependence of the power input and the term U_0^2, respectively. For the conditions examined, it was shown that γ behaved in accordance with the power dependence $\gamma \propto R_\lambda^{-n}$ with $n \approx 0.6$. General expressions were derived to characterise the properties of turbulence in both the internal and external regions. Overall it was suggested that useful estimates of ε could be gained from the expression $\varepsilon/\bar{\varepsilon} = (U^2/\tau_E)/\langle U^2/\tau_E\rangle$ in which the terms $\bar{\varepsilon}$ and $\langle\cdots\rangle$ refer to spatial average values.

Keywords: Multigrid oscillatory mixer; Energy dissipation; Energy balance; Eulerian time scale; Reynolds number

1. Introduction

Since the pioneering work of Rouse and Dodu [1], there has been considerable interest in the use of oscillating-grid turbulence as an alternative to wind-tunnel, grid induced turbulence for studying fundamental properties of turbulence e.g. Voropayev and Fernando [2], or as a means of controlling mixing regimes. Studies such as [3–6] have focused on the spatial decay of turbulence from a single grid. Because turbulence is well-characterised and reasonably homogeneous, away from the immediate vicinity of the grid motion, the oscillating grid has become a valuable tool for studying transport phenomena. A separate development has been the use of stacks of oscillating grids, discs and plates as an alternative to impellers for controlling mixing in reactors. In contrast to the previous group, studies such as [7,8] have provided valuable insight into the power generation, arising from grid movement. Very few studies have taken the step of measuring both the power input and the turbulence. Bache and Rasool (B and R) [9] implemented this approach in a study of the spatial distribution of energy dissipation arising from a single oscillating grid, but their study was restricted to a single level of power input. Useful progress has been made in the combined experimental and theoretical study of Matsunaga et al [10] which attempted to link the character of the turbulence with grid parameters. As with so many studies, there was no direct knowledge of the initial power input. A further aspect is that, most studies tend to focus on the character of the turbulence away from the grid and do not consider the character of the turbulence within the domain swept by the grid. For mixers used in practice, knowledge is generally required throughout the whole mixing domain. For the case of a grid oscillating with low amplitude and relatively high frequency, B and R found that the highest levels of energy dissipation (ε) coincided with the domain swept by the grid.

Taking a broader perspective, it must be recognised that the energy dissipation is an important scaling parameter in the description of isotropic turbulence [11]. As such, it features in many studies such as coagulation kinetics [12] or in the specification of the rupture dynamics of drops and

* Corresponding author. Tel.: +141-552-4400/3351; fax: +141-553-2066.

1385-8947/01/$ – see front matter
PII: S1385-8947(00)00217-5

Nomenclature

A	coefficient in $\varepsilon = Au^3/l$
A_c	cross-sectional area of column (m^2)
C	coefficient in Eq. (11)
C_p	constant in Eq. (5)
C_{u0}	constant in Eq. (24)
d	bar diameter (m)
$E(f_u)$	one-dimensional power spectrum
f	vibrator driving frequency (Hz)
f_u	frequency of u component (Hz)
F	U_{obs}^2/U_0^2
l	integral length scale of energy-containing eddies (m)
L	grid spacing (m)
m	index in equation $\langle R_\Gamma \rangle = C_\Gamma X^m$
m_L	mass of liquid in the column (kg)
n	coefficient in Eq. (2)
n_g	number of grids in column
P_1	average power input per grid ($N\,m\,s^{-1}$)
R_N	fSd/ν, grid Reynolds number
R_S	fS^2/ν, grid Reynolds number
R_λ	$u\lambda/\nu$, microscale Reynolds number
$R_{\lambda 0}$	$U_0\lambda_0/\nu$, microscale Reynolds number in external region
R_Γ	$U^2\tau_E/\nu$, macroscale Reynolds number
$R_{\Gamma 0}$	$U_0^2\tau_{E0}/\nu$, macroscale Reynolds number in external region
S	grid stroke length (m)
u, v, w	rms turbulence velocity in x, y, z directions ($m\,s^{-1}$)
U^2	$(2u^2 + w^2)/3$, average turbulence intensity ($m^2\,s^{-2}$)
U_0^2	scaling value of U^2 defined at extremity of grid stroke length ($m^2\,s^{-2}$)
U_{obs}^2	observed value of U^2 at extremities of grid stroke length ($m^2\,s^{-2}$)
X	defined by $X^m = R_S^{(1+2\beta)(1-n/2)} R_N^{\alpha(1-n/2)}$ (see Eq. (27) and Fig. 8)
x, y, z	orthogonal coordinate frame with x, y in horizontal and z in vertical plane

Greek symbols

Φ_i, Φ_e	parameters defined by Eqs. (22) and (23), respectively
Γ	$(2u^2\tau_u + w^2\tau_w)/3$ ($m^2\,s^{-1}$)
Γ_0	$U_0^2\tau_{E0}$, scaling factor ($m^2\,s^{-1}$)
α	coefficient describing Reynolds number variation in Eq. (5)
β	coefficient describing Reynolds number variation in Eq. (24)
ε	rate of energy dissipation per unit mass ($m^2\,s^{-3}$)
ϕ_i, ϕ_e	spatial distribution functions in the internal, external regions
γ	coefficient in Eq. (1)
γ_0	constant in Eq. (2)
λ	Taylor length scale (m)
λ_0	Scaling value of λ in external region (m)
ν	kinematic viscosity ($m^2\,s^{-1}$)
ρ	density of fluid ($kg\,m^{-3}$)
σ	grid solidarity
τ	λ/U time microscale (s)
τ_E	Γ/U^2 weighted average of Eulerian time integral scale (s)
τ_{E0}	scaling value of τ_E from internal region (s)
τ_u, τ_w	Eulerian time integral scales of u, w components (s)

aggregates suspended in turbulent flows [13–15]. This type of problem demands knowledge of the local rate of energy dissipation and signifies a raison d'etre for this paper. Here, the principal task has been to specify the distribution of the rate of energy dissipation per unit mass (ε) within a multigrid oscillatory mixer and to relate the character of the turbulence to externally controlled parameters such as the grid oscillating frequency (f), stroke length (S) and kinematic viscosity (ν). It makes use of the energy balance approach described in B and R, in which it was concluded that in the domain of the energy containing eddies, ε could be estimated by using a relationship of the form

$$\varepsilon = \gamma \frac{u^2}{\tau_u} \tag{1}$$

In Eq. (1), u is a turbulence rms velocity, τ_u is the corresponding Eulerian time integral scale and γ is a coefficient which was observed in B and R as being independent of distance from the grid. This observation stemmed from the collapse (i.e normalisation) of the measured power spectrum at different distances from the grid. The term γ may be regarded as a form of Reynolds number ($= \varepsilon\tau_u/u^2$). Indeed, in the domain of the energy-containing eddies and where viscous forces cannot be neglected, Hinze [16] notes that there exists a Reynolds number which 'would remain constant during the decay of turbulence'. Similar comments are made by George [17]. Eq. (1) closely resembles the inviscid estimate for the dissipation rate $\varepsilon = Au^3/l$ in which l represents the size of the largest eddies (see [16], p. 20). Here a distinction is made between A and γ on the grounds that one cannot necessarily assume the equivalence $l \equiv u\tau_E$. Nevertheless, for progress, it will be assumed that $l \sim u\tau_E$ and therefore, that $\gamma \sim A$. Experimental data summarised in [18] shows $A \approx 1$ at high Reynolds number whereas at low Reynolds number it was evident that A was correlated with the turbulent Reynolds number $R_\lambda = u\lambda/\nu$ in which λ

refers to the Taylor microscale and ν to the kinematic viscosity. With reference to analysis shown in [19], it seems likely that the coefficient γ can be represented by the function

$$\gamma = \gamma_0 R_\lambda^{-n} \tag{2}$$

in which γ_0 and n are constants. Long's analysis [19] (which was based on the behaviour of $A = l\varepsilon/u^3$) indicated $n \approx 0.4$ and $\gamma_0 \approx 5.6$, the relationship holding for the range $10 \leq R_\lambda \leq 10^4$. At low Reynolds number (say $R_\lambda < 10$), Sreenivasen [18] argued for the case $n = 1$ on the basis of a proportionality between the integral length scale and λ.

At scales smaller than l, and where the turbulence is isotropic, the energy dissipation can be evaluated [20], using the expression

$$\varepsilon = 15\nu\frac{u^2}{\lambda^2} \tag{3}$$

The principal difficulty of using Eq. (3) lies in the evaluation of λ^2. In this analysis, modified forms of Eqs. (1) and (3) will be used to make due allowance for the non-isotropic nature of the turbulence near the grid — particularly at the larger length scales. In addition to the problems of anisotropy, it is necessary to evaluate γ in Eq. (1). This aspect was tackled in B and R on the basis of the energy balance

$$\bar{\varepsilon} = \frac{1}{h}\int_{-h/2}^{h/2} \varepsilon \, \mathrm{d}z \tag{4}$$

in which h refers to the depth of the fluid in a mixing column. The left hand side of Eq. (4) can be determined from the measured power input. Substitution of Eq. (1) into the right hand side permits its evaluation via turbulence measurements, with γ remaining as the only unknown. This form of analysis is elaborated in Section 3.

2. Materials and methods

2.1. Power input

The mixer used in this study is illustrated in Fig. 1. Grids were formed from 1 mm diameter stainless steel wire woven mesh (termed as 'three mesh' i.e. three holes to the inch). The drive shaft assembly on which the grids were mounted was supported by Teflon bearings to minimise friction. A crank assembly provided sinusoidal motion with a maximum stroke of 25 mm and a frequency range of 0.1–3.1 Hz. A series of plane glass windows located in the wall of the mixer allowed turbulence measurements to be gained by laser doppler anemometry, using an externally mounted probe.

The instantaneous forces on the grid were measured, using a Kistler force transducer (Type 9203) located in the driving shaft and were translated into the average power input per grid (P_1) using the procedures described in B and R.

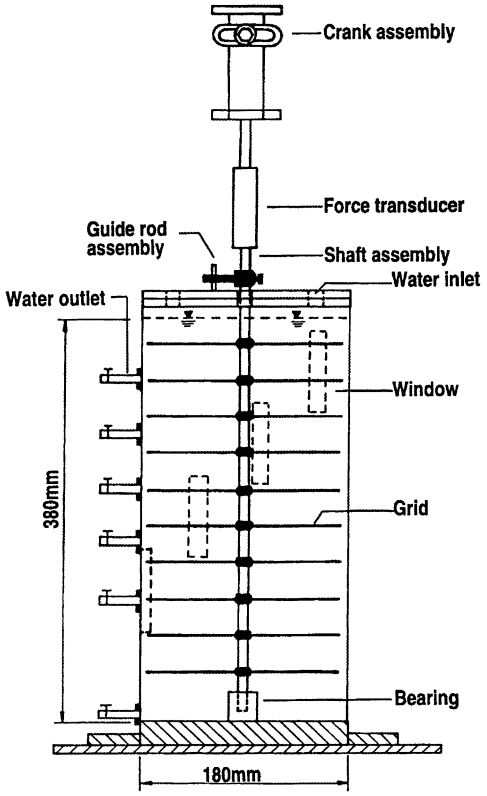

Fig. 1. Schematic design of mixer.

Most readings were based on water at 17–20°C as the fluid medium. Two other sets were gained using aqueous glycerol solution characterised by the density $\rho = 1070\,\mathrm{kg\,m^{-3}}$, $\nu = 4.38 \times 10^{-6}\,\mathrm{m^2\,s^{-1}}$ and $\rho = 1116\,\mathrm{kg\,m^{-3}}$, $\nu = 8.85 \times 10^{-6}\,\mathrm{m^2\,s^{-1}}$. Following B and R, these were collated on the basis of

$$P_1 = C_\mathrm{p}\rho\, A_\mathrm{c}\sigma f^3 S^3 R_\mathrm{N}^{-\alpha} \tag{5}$$

in which C_p is a calibration constant, ρ the fluid density, A_c the overall cross-sectional (area $= 0.0227\,\mathrm{m^2}$), σ the corresponding solidarity (i.e. grid solids area/$A_\mathrm{c} = 0.22$) and α a coefficient which controls the influence of a grid Reynolds number (R_N). The latter was defined by

$$R_\mathrm{N} = \frac{fSd}{\nu} \tag{6}$$

The value of α was obtained by first measuring the power input using water as the fluid and then for a glycerol solution at the same f, S setting. Eq. (5) shows that the relative power change depends on both the viscosity and the fluid density in the form $P_1(\rho_1, \nu_1)/P_1(\rho_2, \nu_2) = (\rho_1\nu_1^\alpha)/(\rho_2\nu_2^\alpha)$. Each pairing yields an estimate of α, a set of tests yielding $\alpha = 0.35 \pm 0.05$ (S.D.). Fig. 2 shows a plot of P_1/ρ versus $f^{3-\alpha}S^{3-\alpha}\nu^\alpha$ at $\alpha = 0.35$ for the entire data set. From this, it was estimated that $C_\mathrm{p} = 97 \pm 22$ (S.E.).

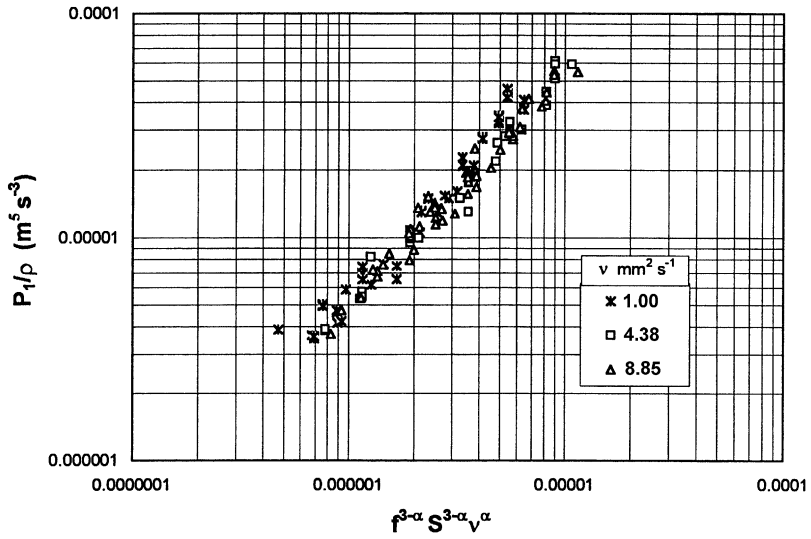

Fig. 2. Plot of power data based on form of Eq. (5) taking account of variations in grid frequency, stroke length, kinematic viscosity and fluid density for $\alpha = 0.35$.

2.2. Turbulence measurements

Turbulence measurements were obtained by using a LDA system (TSI model 9710), comprising a one-component dual beam system with backscatter optics and an IFA-550 signal processor (TSI). Measurements of turbulence were recorded at a sequence of points about 20 mm from the outer wall and at 2 mm height intervals across two sets of three grids within the column. Measurements included the horizontal (u) and vertical rms components (v) and spectral analysis was used to measure the time integral scale of each component. In all the cases, the spectra were rendered noise free by subtracting the background spectrum associated with zero mixing from the total spectrum. The background rms value was in the range of 0.001–0.005 m s^{-1}.

2.2.1. Measurement of τ_E

One dimensional power spectra were obtained via packaged software based on the Fast Fourier Transform technique. The selection of the sample frequency was carried out in accordance with the techniques described in B and R. The shape of the spectra were similar to those reported in B and R and followed a $-5/3$ slope in the higher frequency domain. Two approaches were adopted for determining τ_E In the first, the power spectra were 'cleaned' in order to remove the distorting effect of the driving frequency (and its harmonics) on the time correlation coefficient; $\tau_E$was then calculated from the autocorrelogram. The theory and implications of this procedure have been fully described in [21]. This was a very time-consuming approach as it involved a manual smoothing of the spectral data. In the second approach, the time integral scale τ_u associated with the u component was computed from the intercept of the power spectrum $E(f_u)$ (with f_u as the frequency) using

$$\underset{f_u \to 0}{\text{Lt}}\ \tau_u = \frac{E(f_u)}{4u^2} \tag{7}$$

and similarly for the vertical timescale τ_w: Brumley and Jirka [22] commented that such spectral intercepts can only be considered as rough estimates for the computation ($\pm 50\%$) of the respective time scales. Preliminary analysis showed that there was satisfactory agreement (i.e. within a few percent) between the two approaches. On this basis, all succeeding analysis made use of the intercept approach represented by Eq. (7).

2.2.2. Catering for anisotropy

Initial inspection of the data showed considerable evidence of non-isotropy, particularly in the area swept by the grid. For example, in these regions $w^2 \approx 4u^2$, indicating a greater persistence of the eddy motion along the axis of grid movement. Similarly, it was found that the horizontal and vertical time scales were different. In order to select a representative timescale for inclusion in a three dimensional equivalent of Eq. (1), the following definition was introduced

$$\tau_E = \frac{\Gamma}{U^2} \tag{8}$$

with

$$\Gamma = \tfrac{1}{3}(2u^2\tau_u + w^2\tau_w) \tag{9}$$

and

$$U^2 = \tfrac{1}{3}(2u^2 + w^2) \tag{10}$$

The term U^2 can be regarded as representing the average intensity per component. In both Eqs. (9) and (10), it has been assumed that the horizontal turbulence components

were identical. With these definitions, Eq. (1) can be redefined with the term u replaced by U and τ_E defined by Eq. (8). When the turbulence is isotropic, the modified definition reduces to the form shown by Eq. (1). Following similar logic, Eq. (3) can be recast in the form

$$\varepsilon = C\frac{U^4}{\nu R_\lambda^2} \tag{11}$$

with

$$R_\lambda = \frac{U\lambda}{\nu} \tag{12}$$

For progress, the term C in Eq. (11) is treated as a constant and we recognise the speculative nature of this assumption. The strongest argument in its favour, stems from the self-preserving form of the energy spectrum, this being akin to the remarks by Hinze [16] noted in the introduction. For isotropic turbulence $C = 15$, this following from Eq. (3). In non-isotropic turbulence it is rather difficult to evaluate C. For progress, the value $C \sim 15$ was adopted as a convenient estimate of its magnitude. Later in (Eq. (32)), it will be seen that it is possible to evaluate ε without direct knowledge of C and the assumption is not too critical.

It is also useful to note that the combination of Eq. (1) (in modified form) with Eqs. (8) and (11) leads to the identity

$$R_\lambda^2 = \frac{C}{\gamma}R_\Gamma \tag{13}$$

with

$$R_\Gamma = \frac{\Gamma}{\nu} = \frac{U^2\tau_E}{\nu} \tag{14}$$

3. Analysis

3.1. Base trends

Two representative sets of of data are shown in Figs. 3 and 4 which illustrate the spatial dependence of U^2, τ_E, $U\tau_E$, $U^2\tau_E$, and U^2/τ_E signifying the energy, timescale, length-scale, diffusivity and energy dissipation, respectively for packs of 19 and 10 grids. In the case of the 19 grid data (where every point within the sample range is 'swept' by a grid), the turbulence parameters are reasonably uniform, but with typical scatter. The 10 grid data, spanning the area swept by each of two grids, together with intervening space is of considerable interest. In the zones swept by the grids τ_E is virtually constant, appearing to be unconnected with the U^2 dependence, but increases at distances beyond the stroke amplitude. In contrast, the parameter $U^2\tau_E$ is dominated by the U^2 variation within the stroke distance, but remains essentially constant within the intervening space. It is seen that the length scale $U\tau_E$ increases with distance beyond the stroke domain until the turbulence fields generated by adjacent grids interact. Amongst these spatial variations, the most striking are those associated with the dissipation term U^2/τ_E, which shows that the vast majority of the dissipation is confined to the regions swept by the grid. In contrast, the dissipation within the intervening region is extremely low.

The pattern of $U^2\tau_E$ is of particular interest. Eq. (13) shows that, where $U^2\tau_E$ varies such as in the area swept by the grid (termed as an 'internal' zone), R_λ must also vary. Similarly, in the the domain outside the area swept by the the grid (termed as the 'external' region) where $U^2\tau_E$ is essentially constant, it is deduced that R_λ must also be constant.

3.1.1. Viscosity dependence

A series of measurements were carried out to discern the sensitivity of the turbulence parameters to a change in viscosity, using water at about 20°C ($\nu_w = 1.0\times10^{-6}\,m^2\,s^{-1}$) and a glycerol solution with $\nu_g = 2.0\times10^{-6}\,m^2\,s^{-1}$. In this series, the set of 19 grids was used at the setting $f = 2.05\,Hz$ and $S = 0.018\,m$. To avoid systematic errors, the fluid was swapped at every measuring point, all other conditions remaining identical. It should be remarked that this procedure was very time-consuming, measurement and analysis taking about 2 months. Data showed that $\langle U^2\rangle_{water}/\langle U^2\rangle_{glycerol} \sim (\nu_w/\nu_o)^{-0.20}$ in which the term $\langle U^2\rangle$ refers to the spatial average value. In the case of the timescales $\langle\tau_E\rangle_{water}/\langle\tau_E\rangle_{glycerol} \sim (\nu_w/\nu_o)^{0.13}$. Of the two dependences, the behaviour of $\langle U^2\rangle$ is regarded as the more accurate, the timescale being more prone to error as noted in Section 2.2. In both the cases, the viscosity dependence is fairly small.

3.1.2. Sensitivity to grid motion

The parameters illustrated in Figs. 3 and 4 can also be examined in terms of their spatial average variation. While this approach disguises the spatial variations, it provides insight into the scaling factors which link the character of turbulence to the initial conditions. At this stage, the objective was to discern the dependence of $\langle U^2\rangle$ on f and S. There exist many potential analytical forms for representing the behaviour of $\langle U^2\rangle$. The behaviour of $\langle U^2\rangle$ must be governed by the factors which control U^2. On dimensional grounds, one must expect $U^2 \propto f^2S^2$ as the primary relationship. Many studies include a dependence on the mesh size e.g. Matsunaga et al [10], but few have addressed the potential influence of viscosity, this being encapsulated in a Reynolds number dependence. In the present analysis, a number of empirical forms were postulated to represent U^2 and their consequences in the subsequent analysis was examined in depth. On the basis of such analysis, it was concluded that the underlying scaling of U^2 (excluding mesh geometry) was best represented by $U^2 \propto f^2S^2R_S{}^\beta$ in which β is a constant, the Reynolds number R_S being defined by

$$R_S = \frac{fS^2}{\nu} \tag{15}$$

Using the trial function, the best fit of the $\langle U^2\rangle$ data was obtained with $\beta = 0.25 \pm 0.05$ (S.E.) (see Fig. 5). This

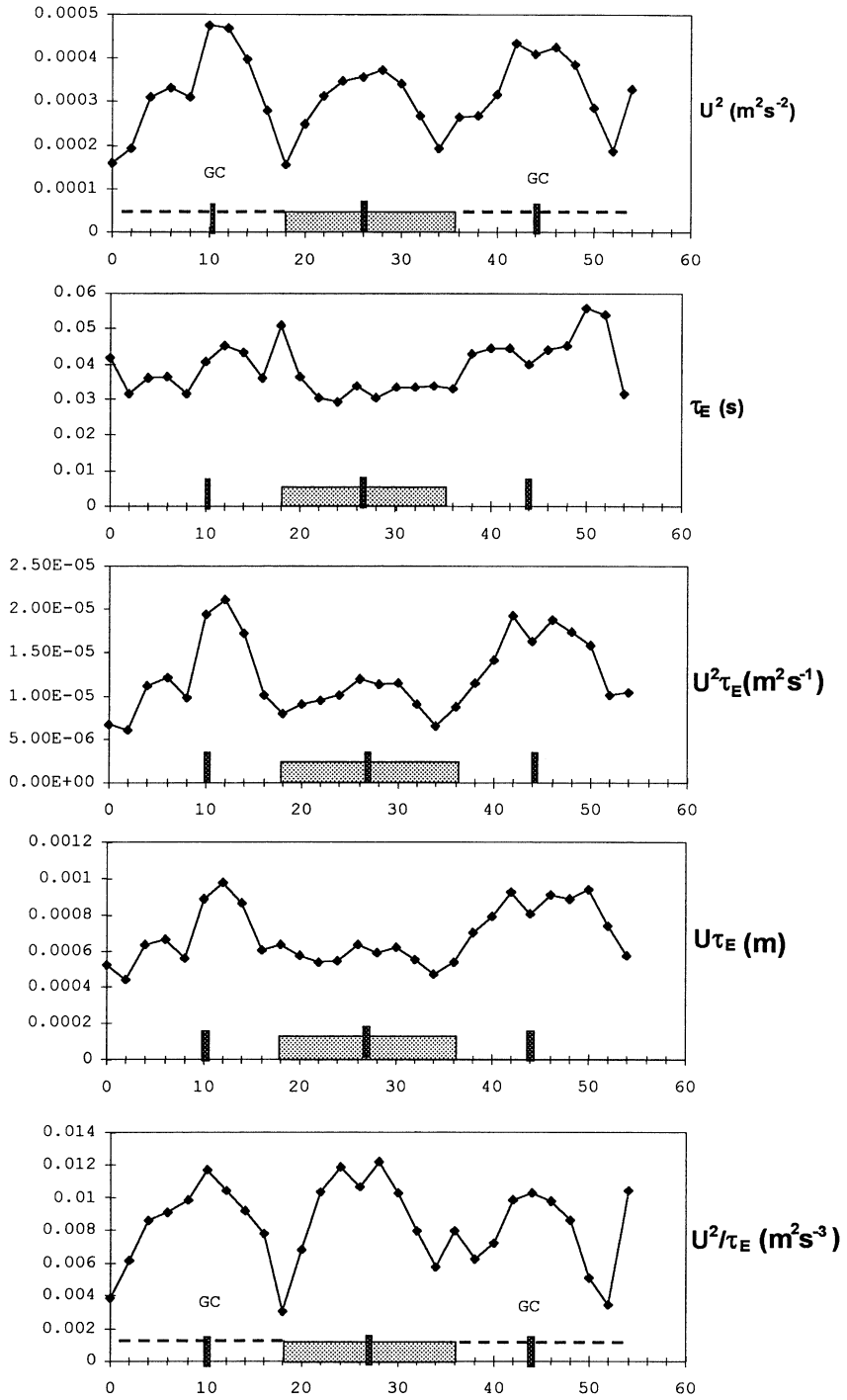

Fig. 3. Plot showing 19 grid data at $f = 2.05$ Hz, $S = 18.17$ mm, $L = 17$ mm. GC refers to the grid centre. The shaded areas signify the zones swept by the grid.

assessment was backed by a multi-regression analysis which showed $\langle U^2 \rangle \sim f^{2.0} S^{2.5(4)}$ in which the index values of f and S are different. This behaviour also fits in with the viscosity dependence ($\langle U^2 \rangle \sim \nu^{-0.2}$) noted above. For the record, we note that the data shown in Fig. 5 was also well-fitted by $\langle U^2 \rangle \propto f^2 S^2 R_N^\beta$ with $\beta = 0.48$; however, the latter relationship does not comply with the observed dependence on changes in viscosity. Further, the form $\langle U^2 \rangle \propto f^2 S^2 R_N^\beta$ implies that the index values of f and S are identical. Again, this did not comply with trends in the data.

3.2. Energy balance

Having measured the power input per grid (P_1), $\bar{\varepsilon}$ follows from the definition

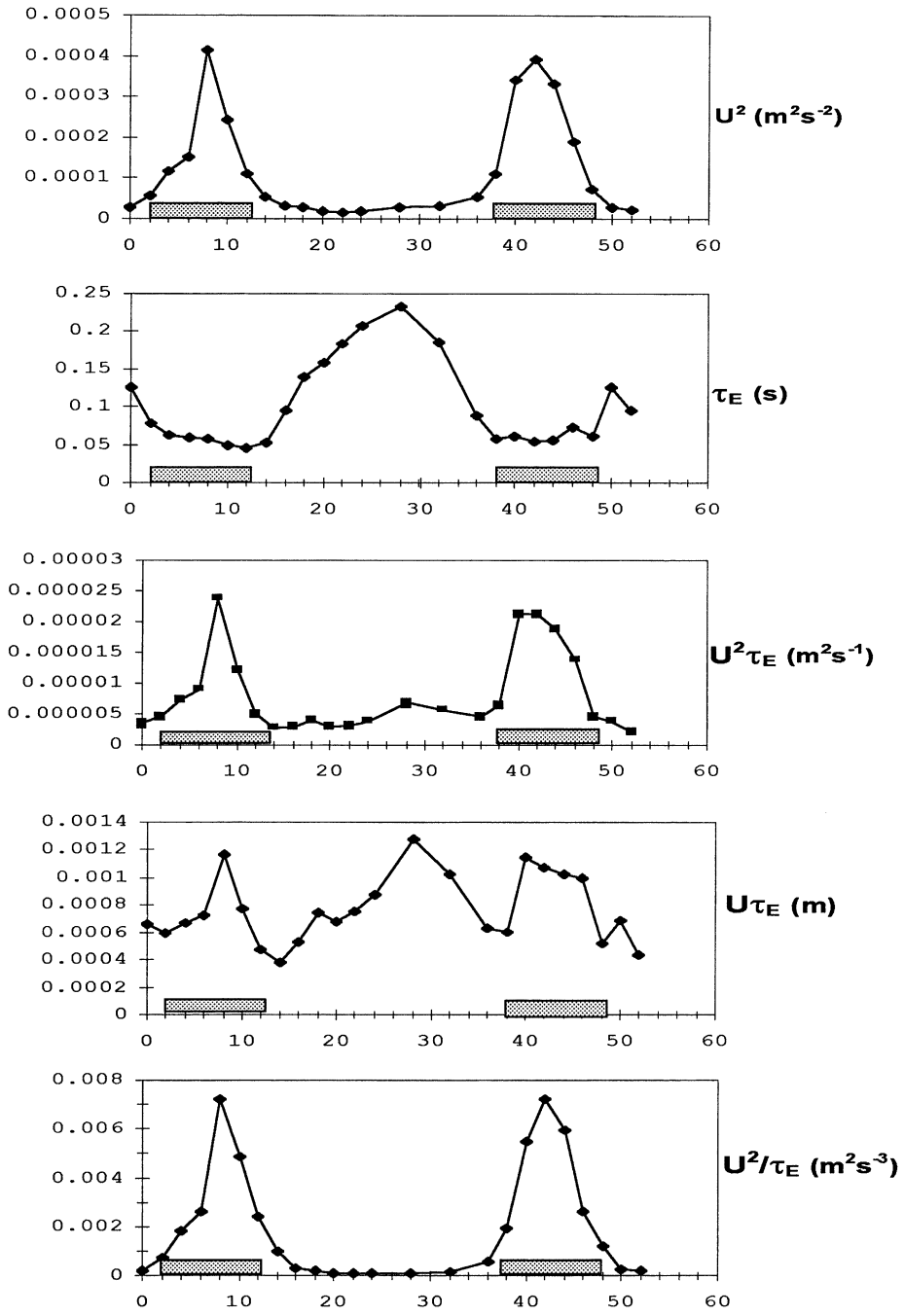

Fig. 4. Plot showing 10 grid data at $f = 2.05\,\text{Hz}$, $S = 12.14\,\text{mm}$, $L = 34\,\text{mm}$. GC refers to the grid centre. The shaded areas signify the zones swept by the grid and are referred to as 'internal' zones.

$$\bar{\varepsilon} = \frac{n_g P_l}{m_L} \tag{16}$$

in which n_g refers to the number of the grids and m_L is the mass of liquid in the column. From this, the energy balance (see Eq. (4)) for the stack is well represented by the statement

$$n_g \gamma \left[\underset{\text{internal}}{\int} \frac{U^2}{\tau_E} \mathrm{d}z + \underset{\text{external}}{\int} \frac{U^2}{\tau_E} \mathrm{d}z \right] = \frac{n_g P_l h}{m_L} \tag{17}$$

The terms 'internal' represents the integration over the domain swept by any individual grid, while the term 'external' refers the integration over the remaining space within the column. On the basis of the behavioural features shown in Fig. 4 and illustrated schematically in Fig. 6, the character of the turbulence can be represented by the following dependencies

Internal:

$$\tau_E = \tau_{E0} \tag{18a}$$

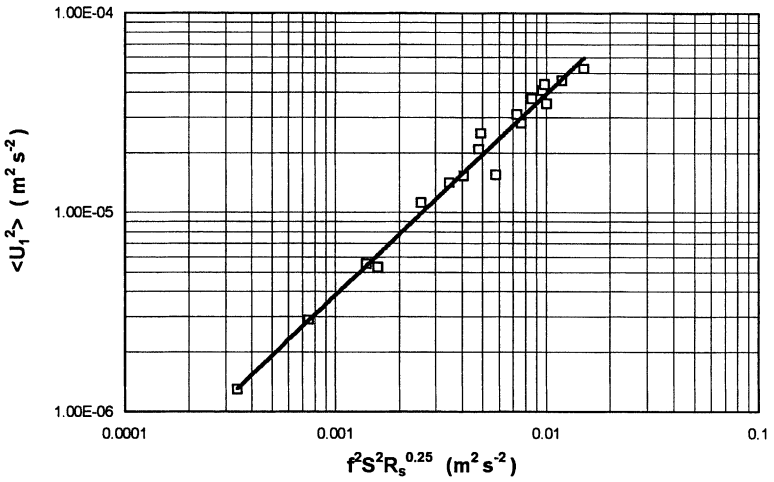

Fig. 5. Dependence of spatial value of turbulence intensity per grid $\langle U_I^2 \rangle$ on the grid velocity scale fS and Reynolds number in the form of Eq. (24) at the best fit value $\beta = 0.25$. NB. $\langle U_1^2 \rangle = \langle U^2 \rangle$/ng.

$$U^2 = U_0^2 \phi_{\mathrm{i}}(z) \tag{18b}$$

External:

$$U^2 = U_0^2 \varphi_{\mathrm{e}}(z) \tag{19a}$$

$$\tau_{\mathrm{E}} = \tau_{\mathrm{E0}} \varphi_{\mathrm{e}}^{-1}(z) \tag{19b}$$

in which τ_{E0} and U_0^2 are reference values of the time scale and turbulence intensity at the common boundary of the regions (say at $\pm S/2$) at which $\varphi_{\mathrm{i}}(z) = \varphi_{\mathrm{e}}(z) = 1$.

In the external region, the paired equations satisfy the observation $U^2 \tau_{\mathrm{E}} = U_0^2 \tau_{\mathrm{E0}}$. This allows Eq. (13) to be written as

$$\gamma = C \frac{U_0^2 \tau_{\mathrm{E0}}}{\nu R_{\lambda 0}^2} \tag{20}$$

in which the Reynolds number $R_{\lambda 0}$ is spatially invariant in this region. Substitution of Eqs. (18)–(20) into Eq. (17) leads to

$$\frac{C U_0^4}{\nu R_{\lambda 0}^2} (\Phi_{\mathrm{i}} + \Phi_{\mathrm{e}}) = \frac{P_{\mathrm{l}}}{m_{\mathrm{L}}} \tag{21}$$

in which Φ_{i} and Φ_{e} refer to the internal and external regions respectively with the schematic definitions

$$\Phi_{\mathrm{i}} = \int_{-S/2}^{S/2} \varphi_i(z)\, dz \tag{22}$$

$$\Phi_{\mathrm{e}} = \int_{-h/2}^{-S/2} \varphi_e^2(z)\, dz + \int_{S/2}^{h/2} \varphi_e^2(z)\, dz = 2 \int_{S/2}^{h/2} \varphi_e^2(z)\, dz \tag{23}$$

By performing a numerical integration of U^2 across the internal zone (where it is clearly defined; as in Fig. 4) and normalising by an estimate of U_0^2, it was shown that $\Phi_{\mathrm{i}} \approx 2.8S$. The evaluation of Φ_{e} is more difficult, because it applies to the whole of the remaining part of the column, and in a multi grid system can only be partially observed in regions which are not swept by grids. Its value can be estimated by assuming the dependence $U^2(z) = U_0^2\ (S^2/4z^2)$ i.e. $U^2 = U_0^2$ at $S/2$ and $U^2 \sim z^{-2}$ as has been frequently observed (see Long [4]). Incorporating this spatial variation into Eq. (23), and integrating shows $\Phi_{\mathrm{e}} = S/3$. Hence one finds that $(\Phi_{\mathrm{i}} + \Phi_{\mathrm{e}}) \approx 3.1S$ or $\Phi_{\mathrm{i}}/(\Phi_{\mathrm{i}} + \Phi_{\mathrm{e}}) \approx 0.9$; this shows that the bulk of the energy dissipation takes place within the regions swept by the grids.

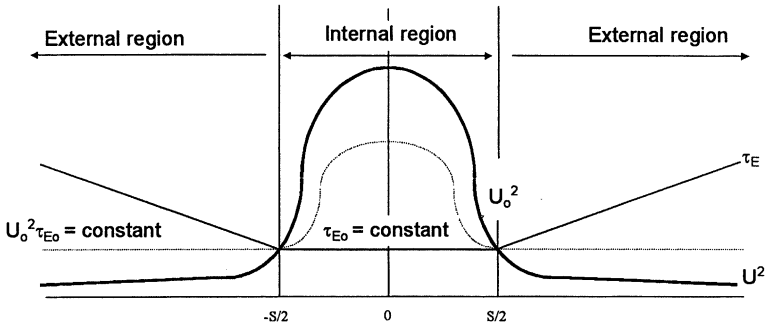

Fig. 6. Description of internal region and external region and schematic form of variation in turbulence parameters.

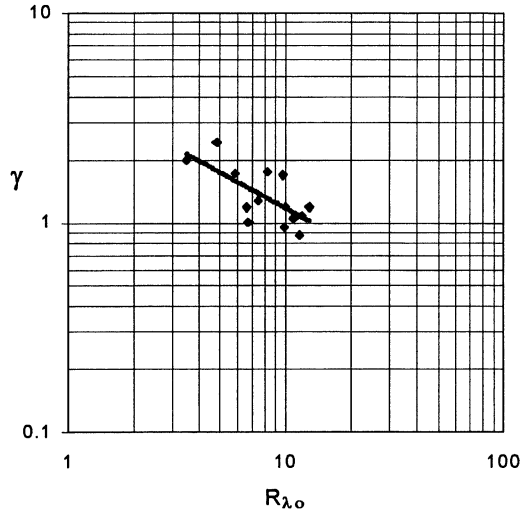

Fig. 7. Sensitivity of parameter γ to Reynolds number $R_{\lambda 0}$. Trend line is $\gamma = 4.3 R_{\lambda 0}^{-0.57}$.

Because the magnitude of $\langle U^2 \rangle$ is dominated by the behaviour of U^2 in the internal region, it can be assumed that the form of U_0^2 complies with the behaviour of $\langle U^2 \rangle$ shown in Fig. 5. Thus, it is suggested that U_0^2 can be represented by

$$U_0^2 = C_{u0} \sigma f^2 S^2 R_s^{\beta} \tag{24}$$

in which C_{u0} is a system constant ($\approx$0.12; this has been estimated from the 10 grid data in conjunction with Eq. (A.1) shown in Appendix A). Note that the form of Eq. (24) must comply with the overall structure of Eq. (21) and accounts for the inclusion of σ. Using Eqs. (5) and (24) to replace the terms P_1 and U_0^4 in Eq. (21), this leads to the definition

$$R_{\lambda 0}^2 = \frac{3.1\, C C_{u0}^2 \sigma}{C_p} R_N^{\alpha} R_S^{2\beta+1} \tag{25}$$

This deduction is important because it relates $R_{\lambda 0}$ to the initial conditions and accounts for the coupling of viscous dependencies within the power input and U^2.

A second view of the energy balance stems from Eq. (4) in the form

$$\gamma = \frac{n_g P_1 / m_L}{\langle U^2 / \tau_E \rangle} \tag{26}$$

Applying Eqs. (25) and (26) to the individual sets of data leads to the plot shown in Fig. 7. It is seen that $\gamma \sim 1$ and decreases with increasing Reynolds number. A fit of the data using Eq. (2) leads to $n = 0.57 \pm 0.13$ (S.E.) and $\gamma_0 \sim 4.3$. Analysis shown below provides an alternative evaluation of n and appears to be less prone to scatter.

3.3. Identity of time scale τ_E

Combination of Eqs. (2) and (12) in conjunction with Eq. (25) leads to expression

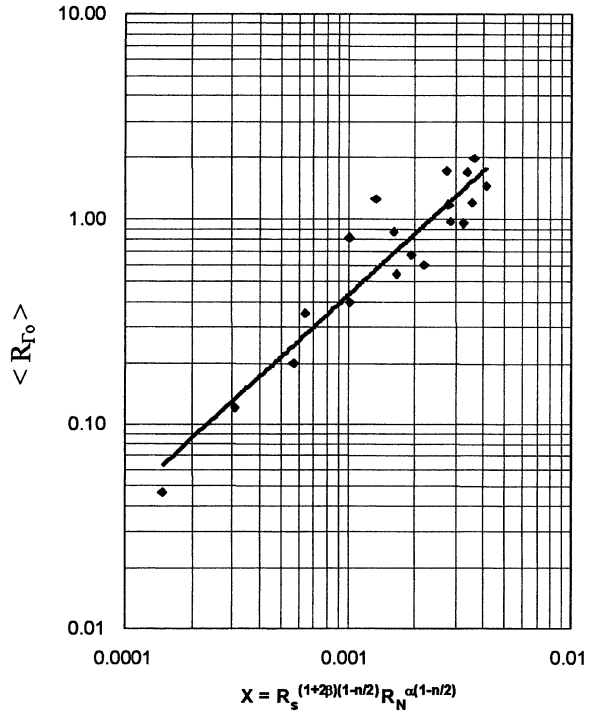

Fig. 8. Based on Eq. (27) in the form $\langle R_{\Gamma 0} \rangle = C_\Gamma X^m$ such that $m = 1$ using $\alpha = 0.35$, $\beta = 0.25$, $n = 0.57$.

$$\frac{U_0^2 \tau_{E0}}{\nu} = C_\Gamma R_S^{(1+2\beta)(1-n/2)} R_N^{\alpha(1-n/2)} \tag{27}$$

By plotting the spatial average $\langle R_\Gamma \rangle$ in the external region in the form of the power function $\langle R_\Gamma \rangle = C_\Gamma X^m$ with X defined by part of the right hand side of Eq. (27) and m an index, may be determined. Parameter n was adjusted by trial and error until a value was reached ($n = 0.57$) corresponding to $m = 1$; i.e. a match between the calculated and observed variations of $\langle R_\Gamma \rangle$. The corresponding plot is shown in Fig. 8. It is seen that both approaches yield the same estimate of n in Eq. (2). Having determined R_Γ, the time scale follows from $\nu\, R_\Gamma / U^2$ i.e.

$$\tau_{E0} \sim \frac{d^2}{\nu} R_S^{[(1+2\beta)(1-n/2)-\beta]} R_N^{[\alpha(1-n/2)-2]} \tag{28}$$

By replacing R_S and R_N by their definitions, the dimensions of the right hand side for the index values of the component term forming the right hand side of Eq. (28) are as follows:

$$f: \quad (1+2\beta)\left(1-\frac{n}{2}\right) - \beta + \alpha\left(1-\frac{n}{2}\right) - 2$$

$$S: \quad (1+2\beta)(2-n) - 2\beta + \alpha\left(1-\frac{n}{2}\right) - 2$$

$$d: \quad \alpha\left(1-\frac{n}{2}\right)$$

$$\nu: \quad -(1+2\beta)\left(1-\frac{n}{2}\right) + \beta - \alpha\left(1-\frac{n}{2}\right) + 1$$

Table 1
General descriptors of internal and external regions

Internal	External
$U^2 = U_0^2 \varphi_i(z)$	$U^2 = U_0^2 \varphi_e(z)$
$\tau_E = \tau_{E0}$	$\tau_E = \tau_{E0}\varphi_e^{-1}(z)$
$R_\lambda = R_{\lambda 0}\varphi_i^{1/2}(z)$	$R_\lambda = R_{\lambda 0}$
$R_\Gamma = R_{\Gamma 0}\varphi_i(z)$	$R_\Gamma = R_{\Gamma 0}$
$U^2/\tau_E = (U_0^2/\tau_{E0})\varphi_i(z)$	$U^2/\tau_E = (U_0^2/\tau_{E0})\varphi_e^2(z)$
$\lambda^2 = \lambda_0^2$	$\lambda^2 = \lambda_0^2\varphi_e^{-1}(z)$
$\tau/\tau_{E0} = (C/\gamma_0)R_{\lambda 0}^{n-1}\varphi_i^{-1/2}(z)$	$\tau/\tau_{E0} = (C/\gamma_0)R_{\lambda 0}^{n-1}$

For example, substituting $\alpha = 0.35$, $\beta = 0.25$, $n = 0.57$ shows

$$\langle \tau_{E0} \rangle \sim \frac{d^{0.25}}{f^{0.93}\nu^{0.07}S^{0.10}} \tag{29}$$

According to this deduction, the time scale exhibits a very weak variation on viscosity, which is consistent with the behaviour reported in Section 3.1. The relationship also indicates that $\langle \tau_{E0} \rangle$ is weakly dependent on S. Regression analysis of $\langle \tau_{E0} \rangle$ against S at fixed f showed $\langle \tau_{E0} \rangle \sim S^{-0.13}$, which is close to the dependence shown in Eq. (29).

3.4. Identity of Taylor microscale

Just as $U_0^2$and τ_{E0} have been defined as scaling factors, one may also introduce the factor λ_0^2 to facilitate the scaling of the λ^2 variation, together with related parameters such as the time microscale $\tau = \lambda/U$. Combination of Eqs. (24) and (25) leads to the definition

$$\frac{\lambda_0^2}{d^2} \sim R_N^{\alpha-2}R_S^{1+\beta} \tag{30}$$

For example, with $\alpha = 0.35$ and $\beta = 0.25$, this leads to dependence

$$\lambda_0^2 \sim \left(\frac{\nu}{f}\right)^{0.4} S^{0.85}d^{0.35} \tag{31}$$

3.5. General descriptors

Table 1 Summarises the principal characteristics of the internal and external region.

4. Discussion

Through the energy balance, it has been shown how the major scaling factors controlling the state of turbulence can be linked to the power input of the grid, the analysis being underpinned by Eq. (1) as a statement of the energy dissipation. A critical feature of the analysis has been the specification of γ. This has been treated as an invariant which permeates the spatial distribution; in doing so, it 'transports' information about the initial conditions. The grounds for this assumption were considered in the Introduction. In the context of the present study, it has led to the development of a framework which is consistent with the observed properties of the turbulence and their response to the initial conditions. Eq. (13) shows that $\gamma \propto R_\Gamma/R_\lambda^2$ i.e. it implies a linkage between the macroscale and the microscale which remains at some fixed value. In the internal region, both R_Γ and R_λ^2 have the same spatial variation, whereas in the external region both are constant. Indeed, it is through the far field dependence that one can specify γ in terms of the Reynolds number $R_{\lambda 0}$ (as in Eq. (20)), $R_{\lambda 0}$ being the only unknown quantity. The evaluation of $R_{\lambda 0}$ stems from Eq. (21) and leads to Eq. (25). It is worth emphasising that Eq. (25) is a statement of the energy balance and shows some crucial links between the character of the turbulence and the initial conditions.

Experimental evidence indicates that the turbulence field can be envisaged as existing in the form of an internal region swept by an individual grid and an external region for distances beyond. When the grids are a sufficient distance apart, these regions are distinct as illustrated in Fig. 4. When the grids are closer together (see Fig. 3), the distributions merge. Although the turbulence generated in the external region by any individual grid is obscured by the turbulence from other grids, its character continues to be 'exerted' through the terms $R_{\lambda 0}$ and γ. Eq. (17) is a conceptual statement which shows the links between single grid and multigrid behaviour, but it must be used with caution. When using multiple grids, Eq. (26) provides a means of estimating γ on the basis of Eq. (1) and is unambiguous statement of the energy balance. However, the key advantage of Eq. (17) is that allows one to dissect the behavioural trends with the terms U_0^2 and τ_{E0} selected as convenient scaling parameters based on single grid behaviour. The form of these parameters are defined through Eqs. (24) and (28), respectively. Although λ_0^2 has been introduced as a scaling parameter, it is not independent of the terms U_0^2 and τ_{E0}. The summary provided in Table 1 provides useful insight into the way in which the character of the turbulence may be specified.

The relative values of the terms Φ_i and Φ_e in Eq. (21) emphasise that 90% of the energy dissipation takes place within the internal region, a feature which can be usefully exploited in order of magnitude calculations. A puzzling feature is the disconnection between U^2 and τ_E in the internal zone. Inspection of Fig. 4 shows that U^2 is at its maximum in the centre of the stroke and least at its extremities, suggesting that it is being driven by the instantaneous velocity of the grid. In the case of the time scale, it is largely a function of the grid frequency as shown in Eq. (29). Its lack of dependence on the stroke length can be explained through Eq. (28), in which the observed value of n (taken as 0.57) is close to the value $n = 0.60$ at which the index of S is zero for the observed α and β.

Most studies of grid turbulence (see De Silva and Fernando [6]) have tended to focus on the character of the turbulence in the external region. Its dominant feature is the constancy of the Reynolds number $R_{\lambda 0}$ as noted in Hopfinger and Toly [5], implying that $\varepsilon \sim U^4/(\nu R_{\lambda 0}^2)$ before the

onset of the final decay. The dependence of the U^2 on the Reynolds number R_S (through Eq. (24)) implies that its sensitivity to f and S *are* different (viz $U^2 \propto f^{2+\beta} S^{2+2\beta}$). This form of behaviour has featured in some studies, e.g. Hopfinger and Toly [5], but generally it must be recognised that these subtle variations and indeed the dependence on viscosity have received scant attention in the previous studies on grid turbulence.

The dependence of the power input on the Reynolds number R_N in Eq. (5) ($\alpha = 0.35$) is well tested. However, it should be regarded as representative of the range of grid Reynolds numbers used in this study and the type of grid which was used. Nevertheless, it is an important parameter because it imparts a viscosity dependence which must be reflected in the character of the turbulence. For example, it is associated with $\beta = 0.25$ in Eq. (24). It is of interest to note that $\alpha + \beta = 0.6$, this closely matching the value of n which provided a best fit of the data shown in Figs. 7 and 8. Whether the match of values corresponding to an identity of the form $\alpha + \beta = n$ is coincidental, or perhaps reflecting an underlying control on the viscosity interdependencies is an aspect which deserves further investigation. Certainly, as the various forms of Reynolds numbers increase i.e. R_N, R_S and R_λ, there must be a tendency towards the inviscid flow description in which α, β and n each tend to zero — a feature which is consistent with the form of the relationship under discussion. Similarly as $R_\lambda \to 0$, $n \to 1$ (as reported in [18]); thus it seems likely that both α and β lie between 0 and 1. It is of interest to note that when $n \to 1$, the combination of Eqs. (13) and (2) shows $\lambda \propto U\tau_E$ whereas at high Reynolds number ($n \to 0$), $\lambda^2 \propto \nu\tau_E$; these show quite different dependencies between the microscale and the macroscale.

When applying the energy balance, it is suggested that Eq. (26) provides the best route for estimating γ for inclusion in Eq. (1). Although Eq. (17) also appears to fulfil the same task, it is a conceptual statement and must be applied with caution when the turbulence fields overlap. The analysis provides clear evidence to show that γ is sensitive to R_λ under the conditions examined, this being represented by Eq. (2) with $\gamma_0 = 4.3$ and $n \approx 0.6$. These values are similar to those reported in [19], but correspond to smaller values of A ($= \varepsilon l/u^3$) around $R_\lambda \sim 10$; this may be due to differences in the specification of the integral length scale l (see Section 1). Without the dependence of γ on R_λ shown by Eq. (2), it would be extremely difficult to match the viscosity dependences of the power input to the characteristics of the turbulence. When γ is treated as a spatial invariant, the combination of Eqs. (1) and (4) lead to the attractive simplification

$$\frac{\varepsilon}{\bar{\varepsilon}} = \frac{U^2/\tau_E}{\langle U^2/\tau_E \rangle} \tag{32}$$

This provides a relatively straightforward means of discerning ε from knowledge of U^2 and τ_E. An Imponderable such as the magnitude of C in Eq. (11) (but treated as constant), cease to be important because it cancels out.

Overall, the energy balance approach appears to offer considerable opportunities for diagnosing the properties of turbulence as well as providing a route for estimating the local average rate of energy dissipation.

5. Conclusions

On the assumption that the factor $\gamma = \varepsilon\tau_E/U^2$ behaves as a spatial invariant, a general framework has been developed to describe the salient properties of the turbulence in terms of the initial conditions.

When the grids were widely spaced, it was evident that the turbulence field was characterised by two principal zones of behaviour. In an internal zone, corresponding to the domain swept by an individual grid, U^2 attained high values compared with other regions and τ_E was essentially constant. Beyond this region, the turbulence was characterised by a constant Reynolds numbers $R_{\lambda 0} = \lambda_0 U_0/\nu$ with λ_0 and U_0 as scaling parameters, the dependence $R_{\lambda 0}^2 \propto \sigma R_N^\alpha R_S^{2\beta+1}$ providing a connection between the properties of turbulence and the initial conditions.

For the conditions examined, it was shown that γ behaved in accord with the power dependence $\gamma \propto \gamma_0 R_\lambda^{-n}$ with $\gamma_0 \approx 4.3$ and $n \approx 0.6$. It was through this relationship that one was able to specify the behaviour of a characteristic Eulerian time scale τ_{E0} in terms of the initial conditions, this being defined via the relationship $U_0^2\tau_{E0}/\nu = C_\Gamma R_S^{(1+2\beta)(1-n/2)} R_N^{\alpha(1-n/2)}$.

On the basis of the spatial invariance of γ, useful estimates of the rate of energy dissipation per unit mass can be gained from the expression $\varepsilon/\bar{\varepsilon} = (U^2/\tau_E)/\langle U^2/\tau_E \rangle$ in which the terms $\bar{\varepsilon}$ and $\langle \cdots \rangle$ refer to spatial average values.

Acknowledgements

This study has been supported at various stages by the Engineering and Physical Science Research Council under GR/F 87134, GR/J 14639; their support is gratefully acknowledged. We are indebted to Professor R.R. Long, currently attached to the Department of Mechanical Engineering and Aerospace Engineering, Arizona State University, Tempe, AZ, USA, for many useful discussions and suggestions on aspects of grid turbulence. We also acknowledge the skills of Mr. T. Towers in the construction of the mechanical equipment used in this study.

Appendix A. Evaluation of U_0^2

The scaling term U_0^2 is tied to its observed equivalent U_{obs}^2 at say $\pm S/2$ (in Fig. 9) for an isolated grid. In a multigrid regime, the turbulence fields will interact unless the grids are

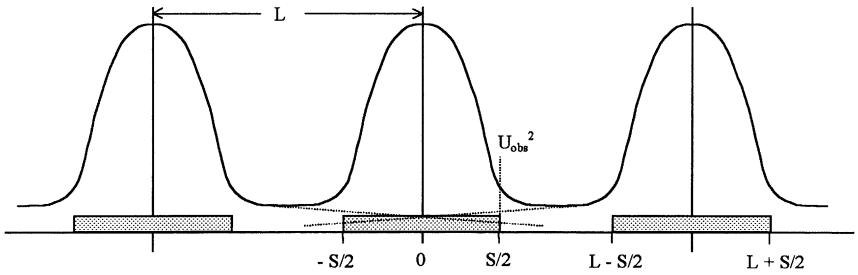

Fig. 9. Schematic layout for calculation of U^2_{obs}.

sufficiently spaced. In order to estimate U_0^2 on the basis of multigrid data, it is assumed that the contributions to U_0^2 are additive, independent, and depend on a decay of the form $U^2 = U_0^2 S^2/4z^2$ in the external region, this satisfying the definition $U^2 = U_0^2$ at $z = \pm S/2$. Under this assumption, the combined influence of a set of grids distance L apart at a reference point $z = S/2$, is simply a summation based on a sequence of origin shifts of the form

$$F = \frac{U^2_{obs}}{U_0^2} = 1 + \frac{S^2/4}{(L - S/2)^2} + \frac{S^2/4}{(L + S/2)^2} + \frac{S^2/4}{(2L - S/2)^2} + \frac{S^2/4}{(2L + S/2)^2} + \cdots \quad \text{(A.1)}$$

Applying Eq. (A.1) to the 10 grid data with $L = 34$ mm and S in the range 10.8–20.7 mm generates F values of 1.07–1.29. Under this scheme ${U_0}^2 = U^2_{obs}/F$.

References

[1] H. Rouse, J. Dodu, Houille Blanche 10 (1955) 522–532.
[2] S.I. Voropayev, H.S.J. Fernando, Phys. Fluids 8 (3) (1996) 2435–2440.
[3] S.M. Thompson, J.S. Turner, J. Fluid Mech. 67 (Part 2) (1975) 349–368.
[4] R.R. Long, Phys. Fluids A 21 (1978) 1887–1889.
[5] E.J. Hopfinger, J.A. Toly, J. Fluid Mech. 78 (Part 1) (1976) 155–175.
[6] I.P.D. De Silva, H.J.S. Fernando, Phys. Fluid A 6 (7) (1994) 2455–2464.
[7] K. Tojo, K. Miyanami, I. Minami, T. Yano, J. Chem. Eng. 17 (1979) 211–218.
[8] M.M. Hafez, M.H.I. Baird, Trans. Ind. Chem. Eng. J. 56 (1978) 229–238.
[9] D.H. Bache, E. Rasool, Chem. Eng. J. 63 (1996) 105–115.
[10] N. Matsunaga, Y. Sugihara, T. Komatsu, A. Masuda, Fluid Dyn. Res. 25 (1999) 147–165.
[11] H. Tennekes, J.L. Lumley, A First Course in Turbulence, MIT Press, Cambridge, MA, 1994.
[12] B.K. Brunk, D.L. Koch, L.W. Lion, J. Fluid Mech. 371 (1998) 81–107.
[13] S. Kresta, Can. J. Chem. Eng. 76 (1998) 563–576.
[14] J. Baldyga, W. Podgorska, Can. J. Chem. Eng. 76 (1998) 456–470.
[15] D.H. Bache, E. Rasool, A. Ali, J.F. McGilligan, J. Water SRT Aqua 44 (1995) 82–92.
[16] J.O. Hinze, Turbulence, 2nd Edition, McGraw-Hill, New York, 1987.
[17] W.K. George, Phys. Fluids A 4 (1992) 1492–1509.
[18] K.R. Sreenivasan, Phys. Fluids 27 (1984) 1887–1889.
[19] R.R. Long, Dyn. Atmos. Oceans 27 (1998) 471–483.
[20] G.I. Taylor, Proc. R. Soc. (London) 151 (1935) 421–478.
[21] E. Rasool, D.H. Bache, Proc. UKALA Colloq., Department of Mechanical Engineering, University of Strathclyde, Glasgow, 7–8 April 1994.
[22] B.H. Brumley, G.H. Jirka, J. Fluid Mech. 183 (1987) 235–263.